Solution and displacement in monolayer and multilayer binary films of SF_6 and CF_4 on graphite

Petros Thomas[a)], Michael D. W. Grogan[b)], and George B. Hess[c)]

Department of Physics, University of Virginia, Charlottesville, Virginia 22904, USA

a)Present address: Department of Chemistry, Kyoto University, Kyoto 606-8502, Japan.
b)Present address: CapitalOne, Richmond, Virginia.
c)Email address: gbh@virginia.edu

Abstract

Infrared reflection absorption spectroscopy is used to study the evolution of binary physisorbed films on graphite. A predeposited monolayer of SF_6 is exposed to slowly increasing pressure of CF_4 at constant temperature between 80 and 113 K. Shifts in the frequencies of the dominant vibrational mode of each species due to resonant dipole-dipole coupling serve as proxies for the areal density of each species in the monolayer. If the initial SF_6 film is far below saturation (coexistence with bulk solid), the SF_6 can be largely displaced by continuous solution of CF_4. However if the initial SF_6 layer is at or near saturation, a layer of CF_4 condenses on top at a well defined CF_4 pressure after only 2-3% dilution of the SF_6 layer. Simultaneously most of the dissolved CF_4 is withdrawn from the SF_6 layer. With further increase in CF_4 pressure, the CF_4 layer is compressed and additional layers condense, while the SF_6 layer is again diluted. Still, the SF_6 layer retains about 90% concentration until the CF_4 pressure is very close to saturation, at which point the SF_6 is rapidly displaced, apparently going into dilute solution in the rapidly growing CF_4 multilayer. Monte Carlo simulations are used to quantitatively relate measured frequency shifts to concentrations in the binary monolayer.

Introduction

The behavior of solutions at solid surfaces at the molecular scale may have relevance in many technical areas, such as nanofluidics, catalysis, electrochemistry, and biological membranes. Films of strongly infrared-active components on a graphite surface may provide useful model systems. There have been a number of experimental studies of binary monolayer to several-layer physisorbed films, many on graphite [For instance, Refs. 1-11 and papers cited there], most of them covering very limited ranges in the relevant three-dimensional thermodynamic space and/or directed at specific features. This is due in part to the difficulty in measuring separately the properties of two components by the commonly used techniques such as volumetry, heat capacity measurement, ellipsometry, x-ray, neutron, electron, or atom diffraction. One feature of particular interest has been the displacement of a strongly bound pre-adsorbed layer by a more weakly attracted second adsorbate. Notable theoretical work includes mean field[12] and Monte Carlo[13] calculations, as well as semi-empirical modeling.

We apply infrared reflection absorption spectroscopy (IRRAS or RAIRS) to study coadsorption of SF_6 and CF_4 on a single graphite (HOPG) surface. This technique allows the partial coverages of both species to be monitored simultaneously. These molecules have dominant vibrational absorption modes at 948 and 1283 cm^{-1}, respectively, and their collective modes in the monolayer are strongly blue-shifted from the free molecule frequencies by resonant dipole-dipole coupling. Thus the monolayer absorption

frequency shift provides a sensitive proxy for the average separation of like nearest neighbors for each species. Because these modes are three-fold degenerate, the molecular orientation has no direct effect on the monolayer frequencies. We have carried out simulations, described below, to quantitatively relate these frequency shifts to the partial densities in the monolayer.

Theory of displacement

If adsorbates A and B are immiscible, displacement of film of A by a film of B occurs as a first-order transition when the spreading pressure of B exceeds that of A. The spreading pressure ϕ at fixed *T* for each phase is given by the Gibbs isotherm relation,

$$\phi(T) = \int_{-\infty}^{\mu} n d\mu' \,, \qquad (1)$$

where $n(T, \mu')$ is the areal density and μ is the chemical potential of the adsorbate. The maximum spreading pressure is attained when the chemical potential μ reaches its saturation value μ_0, at which point a bulk condensed phase begins to form. The chemical potential of each component is given by $\mu = \mu_0 + T\, ln(p/p_0)$, where p is the partial pressure of the 3-D vapor (treated as an ideal gas) in equilibrium with the film. The reference pressure $p_0(T)$ is taken to be the saturated vapor pressure. In this paper, all chemical potentials will be specified relative to saturation, so we take $\mu_0 = 0$.

If A and B are partially miscible, the right side of Eq.(1) will have a second integral for the other component. If A and B are completely miscible, displacement can proceed by continuous substitution. A limiting case of continuous displacement has been analyzed by Weber and Goodstein[8].

Equation (1) with upper limit $\mu_A = 0$ describes displacement of A to bulk liquid or solid. Component A also could be displaced to other reservoirs. If the adsorbent surface-area-to-cell-volume ratio is not too large and the saturated vapor pressure of A is not too small, A could be displaced to 3-D vapor without reaching saturation. Below we consider another scenario, in which a SF_6-rich monolayer is continuously displaced to a dilute solution in a growing overlying multilayer CF_4 film.

The spreading pressure of pure SF_6 can be evaluated by integrating Eq. (1) with the coverage data of Ref. 14, giving at saturation $\phi_{SF6} = 38.4$ K/Å^2 at $T = 110$ K or 38.2 K/Å^2 at 90 K. There may be uncertainty as large as ±1 K/Å^2 due to extrapolation of the condensation chemical potential to low temperatures. At low temperatures the SF_6 monolayer is registered with the graphite substrate and in this case can transfer lateral stress to the substrate, inhibiting or delaying displacement.

The spreading pressure of the pure CF_4 film is estimated from data of Ref. 15 to be 30.0 K/Å^2 at condensation of the second layer ($\mu \approx$ -72 K) and about 38.3 K/Å^2 at saturation. Thus the spreading pressure criterion suggests that displacement may be marginally possible at saturation, but only ignoring any CF_4 layers that condense on top of the SF_6-rich layer.

Experimental Technique

The apparatus has been described previously[14, 18]. Briefly, the HOPG substrate is mounted on a cold finger in a cell that is also cooled (generally a few degrees warmer than the substrate). Windows are provided for reflection of infrared at 70˚ incidence from one side of the substrate and for visible light reflection for ellipsometry at 45˚ incidence on the other side. The temperature is monitored by a diode thermometer attached to the cold finger outside the cell, corrected for an offset determined from the measured saturated vapor pressure of one or both adsorbates. IR spectra are measured with a Mattson

Research Series Fourier transform spectrometer at 1 cm^{-1} nominal resolution. In order to separate surface from gas-phase absorption, the polarization is modulated to extract the difference between p- and s-polarized reflectance. Spectra are usually taken continuously with 2-minute averaging. The ellipsometric signal monitors essentially the total film thickness and is recorded at 5 s intervals, along with the temperature and pressure.

The experiments reported here extend from 80 to 113 K. At each temperature we establish a monolayer of SF_6, usually compressed to saturation. We then admit CF_4 slowly, over several hours, until reaching CF_4 saturation. Finally we study reversibility by cracking open a small valve to the turbo-pump to slowly pump out the CF_4.

Over this temperature range the saturated vapor pressure of CF_4 (0.070 to 36 Torr[16]) is much larger than that of SF_6 (1.4E-7 to 0.006 Torr[17]). Hence the pressure measured over mixed films usually is essentially that of CF_4. The resolution of our pressure gauge (MKS Model 627, 1T) is about 0.01 mT. However in the low milliTorr range the SF_6 partial pressure in the mixture in the cell can be estimated from the area of the gas phase absorption peak at 948 cm^{-1} in the s-polarization (background) spectrum. Thus, under conditions of equilibrium between the film and 3-D vapor, we can determine the chemical potentials of both components, giving a complete specification of the thermodynamic state of the film.

We previously reported studies of pure SF_6 and CF_4 films on graphite using the same techniques.[14,15] Pure SF_6 forms only a single monolayer on graphite before condensation of bulk[14]. The monolayer is 2×2 commensurate with hexagons of the graphite surface below 95 K at saturation or 70 K at layer condensation. At higher temperatures there are two expanded incommensurate solid phases and liquid exists above a triple point at T = 150 K. It is not clear where SF_6 melts in the mixed film. The CF_4 film on bare graphite grows up to a bilayer at temperatures below 72 K and to many layers at and above a wetting transition near 90 K. The initial monolayer is liquid above 76 K and compresses to various solid phases. Above about 95 K the CF_4 film remains liquid at all coverages[15].

Experimental Results: CF_4 over a Pre-Adsorbed SF_6 Monolayer

Figure 1 is a typical polarization-modulation spectrum in a region where a single CF_4 layer overlies an SF_6 monolayer. The two peaks from the film are narrow and can be located with considerable precision. A band near 1283 cm^{-1} is noisy because the CF_4 gas in the cell is becoming opaque there, so that the intensities of both polarizations approach zero. Dilute CF_4 peaks in this region will not be observable. If particles of bulk SF_6 were present on the surface, they would contribute a broad hump (FWHM ~ 60 cm^{-1}) centered around 980 cm^{-1}.

Figure 2A is the ellipsometric record for a run at T = 100.6 K, showing the total number of layers during slow increase and then decrease of CF_4 pressure, starting with a monolayer of SF_6 slightly below saturation. Figure 2B shows the vibrational mode frequencies during this run. The starting point near the left axis represents a pure SF_6 monolayer at a partial vapor pressure of about 0.2 mT. As CF_4 is admitted, the SF_6 frequency is seen to decrease from the initial 1003.36 cm^{-1} to 1002.42 cm^{-1} at a CF_4 pressure of 0.84 T. Model calculations, discussed below, indicate that this corresponds to dilution of the SF_6 monolayer by about 1.7 %. No absorption peak due to the minority CF_4 component is observable at this concentration due to proximity to the absorption band of CF_4 gas in the cell. At 0.84 T there is a monolayer-size step in the ellipsometric signal and a new absorption peak appears near 1317 cm^{-1}, indicating condensation of a second layer that is predominantly CF_4. The CF_4 chemical potential at which this step occurs, $\mu \approx$ -196 K, is nearly constant over 90 K < T < 113 K so long as SF_6 is near saturation. This is intermediate between the condensation chemical potential of the first layer (~-660 K) and the second

layer (~-72 K) of pure CF_4[15,19]. Simultaneously the SF_6 frequency jumps up to a value that is comparable to the initial value or higher, indicating that most of the dissolved CF_4 has been pulled back out of the original layer, an effect reported previously[20]. However, at 100.6 K the final frequency is higher than the initial frequency for pure SF_6, so something additional is involved.

Similar behavior was found in all runs above 80 K for which SF_6 was at or very near saturation. Figure 3 summarizes the characteristic SF_6 frequencies *versus* temperature of these three points: (A) Initial pure SF_6; (B) just before step; (C) just after step. The initial pure SF_6 line is in fairly good agreement with results of Thomas *et al*.[14] for saturated SF_6. (Our points at 95.4 and 100.6 K may be slightly below saturation). At the three lowest temperatures the initial film should be 2×2 commensurate with the graphite hexagons, while the higher temperature points should be in the IC1 incommensurate solid phase[14]. The "pre-step" line falls below the "initial" line by an amount increasing with temperature (except at 95.4 K), consistent with solution of an amount of CF_4 that increases with temperature, reaching about 3% at 113 K. The "post-step" line behaves differently, lying 0.4-0.5 cm^{-1} below the "initial" points in the commensurate region, but then continuing almost flat out to 106 K. Beyond 106 K it drops rapidly, going again below "initial" beyond 110 K. The depression relative to pure SF_6 in the commensurate region can be attributed to the stronger image field if the SF_6 layer is pressed about 0.2 Å closer to the substrate by the overlying CF_4. The SF_6 layer then would also see a stronger substrate lateral potential, which we conjecture might extend its commensurate phase to higher temperatures.

Beyond the second-layer step in Fig.2, ν_{CF4} for the (presumed) upper layer increases due to compression in a manner qualitatively similar to the pure CF_4 film, while ν_{SF6} from the bottom layer decreases gradually due to resumed solution of CF_4. Absorption peaks from the minority components are not detected above noise. Additional layers condense at p = 4.34, 5.22, and 5.62 T, producing steps in ν_{CF4} and (in the first two cases) small positive offsets in ν_{SF6}. At about p = 5.8 T (with about seven total layers), ν_{SF6} begins to decrease rapidly and the peak weakens and disappears. Figure 4 is a time plot of the area of the spectral peak associated with SF_6 in the first layer, together with the total number of layers, approaching and leaving CF_4 saturation. This is for a run at 111.1 K in which SF_6 was initially just slightly below saturation; displacement occurs at the fifth layer. Similar displacement is observed at all temperatures above 95 K. Thus there is a different mode of displacement of the SF_6-rich layer as CF_6 approaches saturation.

Following the disappearance of SF_6 from the original layer, a new narrow absorption peak appears and grows at 939 cm^{-1}. This is very close to the frequency reported for dilute SF_6 in 3-D liquid nitrogen and in solid argon[21, 22]. We believe this indicates that the SF_6 has dissolved in the multi-layer, quasi-bulk CF_4. Figure 5 is a time plot of the area of the 939 cm^{-1} absorption peak, together with a plot of the total number of layers from ellipsometry, starting before closing of the leak valve (at t=29500 s) and continuing beyond the start of pumping (at t=31200 s). The area of the 939 cm^{-1} peak is seen to be very nearly proportional to the effective number of layers in excess of seven. A concentration of roughly 3% would account for the amount of SF_6 displaced. A further observation is that the partial pressure of SF_6 dips (by a factor of three in this run) over the same time interval, as shown in Fig. 6. The implied reduction in SF_6 chemical potential is about -145 K. Presumably this SF_6 also goes into the thick CF_4 film.

The saturated vapor pressure of SF_6 is 0.20 mT at 100 K and 3.6 mT at 111 K. Evaporation of a monolayer of SF_6 from the full surface area of the HOPG sample would raise the pressure in the cold cell by very roughly 0.1 mT. Therefore, at least at the lower temperatures, if the pre-adsorbed SF_6 layer is only a little below saturation, the surface SF_6 can be compressed to saturation with only a small amount displaced to vapor. (The actual situation is more complicated because there is presumably also a film reservoir of SF_6 on the larger area of the copper sample mount, which is believed to be less strongly

binding than graphite; thus SF_6 may be displaced from copper to maintain full coverage on graphite during compression). On the other hand, if the initial chemical potential of the SF_6 monolayer is sufficiently below saturation, the maximum spreading pressure will be reduced by allowing complete displacement to 3-D vapor without reaching saturation.

We made two runs at T = 111.3 K with initial SF_6 far below saturation, at chemical potentials of μ_{SF6} = -348 K and -562 K. Results from the first of these runs are shown in Fig. 7. The SF_6 concentration is strongly depleted (to about 35%) prior to the second step, which has moved up to μ_{CF4} = -146 K as a result of the increased CF_4 concentration in the underlayer. Thus both CF_4 and SF_6 absorption peaks from the monolayer could be measured over a significant range. At the second step, the SF_6 concentration in the bottom layer recovered to ~98 %, only to be depressed again to the 35 % range near μ_{CF4} = -65 K and then to undetectable level near -10 K. No separate CF_4 peak from the first layer is seen during this second displacement, indicating that CF_4 in the first layer couples strongly to CF_4 in the second layer. On slowly pumping off CF_4 (not shown), the density of SF_6 in the monolayer recovered, but only very slowly.

In the second run, at initial μ_{SF6} = -562 K, SF_6 in the monolayer is continuously diluted to ~30 % by μ_{CF4} = -300 K, beyond which the SF_6 peak broadens and is lost. The second step has moved up to -109 K. In this case the SF_6 concentration in the bottom layer did not recover significantly at the second step. Slow pump out was started slightly past the second step and the trajectories were found nearly reversible.

Adding SF_6 over monolayer CF_4

One run at T = 80.3 K was started with pure CF_4 at μ = -68 K, just below second layer condensation. On slow admission of SF_6, ν_{CF4} decreased continuously from 1329.6 to 1327.1 cm^{-1}, indicating solution of about 4 % of SF_6 in the CF_4 monolayer. At this point the ellipsometric signal showed condensation of a second layer (over several minutes), and after several minutes delay an SF_6 peak first became visible (at about 999.8 cm^{-1}). Owing to the very low vapor pressure of SF_6, there might be significant delay between condensation on the two sides of the substrate. The SF_6 peak area reached monolayer size in about 30 minutes, while ν_{SF6} increased more slowly, reaching 1003.9 cm^{-1} after two hours. This suggests slow organization of a predominantly SF_6 layer after more rapid deposition of SF_6 in less ordered form, perhaps involving other cold surfaces in the cell. During this process the CF_4 peak area remained fairly constant and ν_{CF4} stabilized near 1326.5 cm^{-1}. The final state can be compared to the state reached by the usual procedure of adding CF_4 over an SF_6 monolayer, where at the same temperature and CF_4 chemical potential we found ν_{CF4} to be 0.2 cm^{-1} lower and ν_{SF6} 0.2 cm^{-1} higher. We could not measure the SF_6 chemical potential at this temperature. On subsequent pumping of the CF_4, ν_{SF6} increased to 1004.37, consistent with a commensurate monolayer. This increase probably represents loss of about 1% of CF_4 previously dissolved in the SF_6 layer.

Simulations

We have carried out simulations to estimate how the frequencies depend on assumed concentration in model SF_6-CF_4 monolayer mixtures. Similar simulations have been reported by Tsyganenko *et al.*[23] for different molecules on a square lattice. A 10×10 rhombus of sites on a triangular lattice is populated randomly with x type-A molecules (SF_6) and $(100-x)$ type-B molecules (CF_4), assigning to each polarizability parameters taken from modeling of the respective pure monolayers[14,15.] This rhombus is then replicated periodically to fill a 21×21 superlattice. The surface-normal component of the electric field at each site $\{i,j\}$ in the original rhombus due to a unit surface-normal dipole at any other site $\{k,l\}$

and each of its replicas is calculated, including a continuum approximation for dipoles beyond the superlattice. This gives 100 simultaneous linear equations for the response to a uniform surface-normal (IR) electric field[24]. These are solved for frequencies from 900 and 1400 cm^{-1} at 0.1 cm^{-1} increments for each of 66 or 132 values of *x*. For each *x*, the frequency of the largest spectral peak in the neighborhood of 1000 cm^{-1} (SF_6) and of 1300 cm^{-1} (CF_4) is tabulated.

The frequency shifts depend not only on the concentration but also on the distribution of the components. To allow a preference for *like* or *unlike* nearest neighbors, the initial random distribution in the base rhombus was modified by repeatedly swapping a randomly selected pair with probability depending on the resulting change in the number of *unlike* neighbors times Δ/T, where

$$\Delta = E_{AB} - \tfrac{1}{2}(E_{AA} + E_{BB}), \qquad (2)$$

and E_{XY} are the nearest neighbor interaction energies. To approximate a thermal distribution, the swapping probability was set to be

$$P = \tfrac{1}{2}\,(1 - \tanh(n\Delta/T)), \qquad (3)$$

where *n* is the resulting increase in the number of *unlike* nearest neighbors. To estimate Δ from experimental data for the mixed monolayer, it is useful to plot v_{CF4} against the corresponding v_{SF6} for the range of compositions. Figure 8 is such a plot for fixed lattice constant a = 5.03 Å and six values of Δ/T. Each line is a fit to the calculated points, which scatter due to the limited size of the computation cell. Symbols are experimental data from the two runs in which both frequencies could be measured in the monolayer. The heavier line is for random distribution (small Δ/T). The best fit to experiment is found for $\Delta/T \approx +0.26$. The assumption that the distribution of molecules depends on only the single parameter Δ/T corresponds to the model of a "regular" solution.

Lattice constant a = 5.03 is the middle of the range for pure solid SF_6 at 111 K[14]. As the CF_4 molecule is slightly smaller, a is expected to decrease with increasing CF_4 concentration. Diagrams like Fig. 8 calculated for other values of a are quite similar except for re-scaling of the axes. The lowest frequency for each constituent is essentially the singleton frequency, 930 cm^{-1} for SF_6 and 1261 cm^{-1} for CF_4, and is insensitive to the lattice constant. The highest frequencies correspond to the pure monolayer of each constituent at an appropriate chemical potential. Thus it should be a reasonable approximation to start with a plot for fixed a and rescale each axis to the appropriate limits. We have started with a set of simulations similar to Fig. 8 for a = 4.92 Å and re-scaled to give a maximum frequencies for SF_6 of 1000.0 cm^{-1} and for CF_4 of 1328.3 cm^{-1}, the frequency of the pure CF_4 monolayer at T = 111 K extrapolated to $\mu = \mu_0$. The best fit gives the revised estimate $\Delta/T = +0.21$, or Δ = 23 K. Figure 9 shows the frequencies *versus* concentration for the re-scaled simulations and $\Delta/T = +0.21$. The asymptotic slope for dilution of SF_6 is -0.58 cm^{-1}/% and for dilution of CF_4 is -0.62 cm^{-1}/%. Based on this calibration, the experimental data in Fig. 8 range from 36 to 70% SF_6.

The v_3 mode of SF_6 hybridizes with the combination mode $v_2 + v_6$ near 991 cm^{-1} to produce an anti-crossing. In the simulations in Figs. 8 and 9 we calculate the unhybridized v_3[14], and the experimental points in Figs. 8. are corrected accordingly[14]. Otherwise we report experimental frequencies, which are about 1.9 cm^{-1} larger than the unhybridized v_3 for $v > 1000$ cm^{-1}.

Conclusions.

When an initial monolayer of SF_6 at or near saturation is exposed to CF_4 vapor, a small amount of CF_4 dissolves in the layer, reaching up to 3% (at T = 113 K) when $\mu_{CF4} \approx$ -196 K. At this point a layer of CF_4

condenses on top (presumably) of the SF_6 layer. This is well below the chemical potential, $\mu_{CF4} \approx -72$ K, at which a second layer condenses on top of a CF_4 monolayer, reflecting stronger van der Waals attraction to the underlying layer when it is SF_6 rather than CF_4. This is accompanied by a positive step in ν_{SF6}, especially for $T > 90$ K, indicating that most of the dissolved CF_4 is abruptly removed from the bottom layer. As the bottom layer remains in equilibrium with only incrementally modified 3-D vapor, this must be driven by interactions between the layers.

On the other hand, if the initial chemical potential of the SF_6 monolayer is far below saturation, replacement of SF_6 by CF_4 can proceed much farther, to at least 65%, with the displaced SF_6 going to 3-D vapor. From the point of view of Weber and Goodstein[8], reduced spreading pressure of the SF_6 monolayer allows more progress toward its complete displacement. At the same time the increasing CF_4 concentration in the monolayer delays the condensation of the second layer that eventually interrupts the process (e.g., to $\mu_{CF4} \approx -109$ K, for $\mu_{SF6} \approx -104$ K and $T = 111.3$ K).

Comparison of the frequencies ν_{CF4} and ν_{SF6} for the mixed monolayer with simulations allows us to estimate the parameter Δ [Eq. (2)], which is relevant to modeling the thermodynamics of solution in the monolayer. We find $\Delta \approx 23$ K; the positive value means like nearest neighbors are energetically favored and solution is driven entirely by entropy. The simulations then provide a calibration for the rate of frequency shift with concentration. In the context of regular solution theory on a 2-D hexagonal lattice[25], phase separation in the monolayer is expected if $T < 3\Delta \approx 69$ K, below the temperature range of the present study.

The reverse procedure, admitting SF_6 over a CF_4 monolayer, was attempted only at 80.3 K. The initial CF_4 chemical potential allowed only a monolayer on bare graphite, but is appropriate for a second layer over an SF_6 monolayer. Development of the SF_6 layer was very slow, presumably due to its low vapor pressure, but the final state was close to that attained in the direct procedure.

When the initial SF_6 layer was at saturation or sufficiently close to be compressed to saturation, we saw solution of only a few per cent of CF_4, thus no substantial displacement of the SF_6 layer, up to CF_4 pressures very near saturation. This is consistent with expectation based on the calculated spreading pressures of a pure CF_4 film and of an SF_6 monolayer with the observed CF_4 overlayers. However for $T >$ 93 K and very close to CF_4 saturation ($\mu_{CF4} \approx -1$ to -7 K), when the film thickness exceeded about five to seven layers, the concentrated SF_6 layer was rapidly displaced and after a delay a new peak appeared at 939 cm^{-1}, which we interpret as dilute SF_6 in quasi-3-D CF_4. We attribute this displacement to the availability of this new reservoir, the multilayer film of liquid CF_4. The spreading pressure criterion applied to the overall film is ambiguous, as the SF_6 remains in the film. The transient state of the SF_6 is not entirely clear. Concurrent with displacement, the SF_6 vapor pressure starts to *decrease*, so SF_6 cannot be going to 3-D vapor or solid. If it goes initially to small clusters in the growing film, the resulting spectrum would be broad and difficult to resolve from background.

We do not resolve a spectral peak due to the CF_4 minority component in a monolayer until its concentration becomes quite large, of order 30%. Fig. 9 shows that the monolayer CF_4 peak is below the free molecule resonance up to a concentration of about 19%, because the resonant dipole blue shift is weaker than the self-image red shift. Under typical conditions the gas is sufficiently opaque that a surface peak could not be resolved below about 1290 cm^{-1}, or almost 30% concentration. Apart from this, the simulations show considerable scatter due to fluctuations in clustering on a local scale, which together with concentration fluctuations could contribute to broadening in the experiment. At sufficiently high concentrations this will be countered by the global tendency of resonant dipole coupling to narrow the collective mode peak (i.e., when the resulting shift is large compared to the

fluctuations).[23] For dilute SF_6 the broadening effect would be similar, but opacity of the vapor is much less significant.

Acknowledgments

This research was supported in part by National Science Foundation (NSF) Grant No. DMR0305194 and by the Physics Department of the University of Virginia. Exploratory measurements on this system were made in our lab by Todd Hopkins and Yu Xia. John Liljegren wrote a user interface for the simulation program. We thank Prof. Ian Harrison and an anonymous referee for their suggestions on the manuscript.

References

1 J. H. Singleton and G. D. Halsey, Jr., J. Phys. Chem. **58**, 1011 (1954).

2 M. Bouchdoug, J. Menaucourt, and A. Thomy, J. Phys (France) **47**, 1797 (1986).

3 J. Menaucourt and C. Bockel, J. Phys (France) **51**, 1987 (1990).

4 M. Abdelmoula, T. Ceva, B. Croset, and N. Dupont-Pavlovsky, Surf. Sci. **272**, 167 (1992).

5 J. Menaucourt, J. Phys. I (France) **3**, 1201 (1993).

6 H. Asada, M. Nishizaki, and Y. Morizawa, Surf. Sci. **383**, 277 (1997).

7 H. Asada, S. Kataoka, K. Takemura, M. Shimada, A. Ikeda, and N. Hamada, Surf. Sci. **443**, 287 (1999).

8 W. J. Weber and D. L. Goodstein, Phys. Rev. Lett. **83**, 3888 (1999).

9 W. J. Weber and D. L. Goodstein, Phys. Rev. B **66**, 165419 (2002); **73**, 195424 (2006).

10 P. Thomas, D. Velazquez, and G. B. Hess, J. Chem. Phys. **134**, 114702 (2011).

11 M. J. Retamal, M. A. Cisternas, S. E. Gutierrez-Maldonado, T. Perez-Acle, B. Seifert, M. Busch, P. Huber, and U. G. Volkmann, J. Chem. Phys. **141**, 104201 (2014).

12 F. Hommeril and B. Mutaftschiev, Phys. Rev. B **40**, 296 (1989); Croatica Chemica Acta **63**, 489 (1990).

13 K. Grabowski, A. Patrykiejew, and S. Sokolowski, Surf. Sci. 506, **47** (2002) and references cited there.

14 P. Thomas, Y. Xia, D. A. Boyd, T. A. Hopkins, and G. B. Hess, J. Chem. Phys. **131**, 124709 (2009).

15 P. Thomas and G. B. Hess, J. Chem. Phys. **140**, 194703 (2014).

16 B. Genot and X. Duval, J. Chim. Phys. 67, 1332 (1970); L. Q. Lobo and L. A. K. Staveley, Cryogenics **19** (1979)

17 B. Genot, J. Chim. Phys. 68, 111 (1971).

18 T. A. Hopkins, D. A. Boyd, Y. Xia, G. M. Shifflett, F. M. Hess, and G. B. Hess J. Chem. Phys. **128**, 154714 (2008).

19 H. S. Nham, M. Drir, and G. B. Hess, Phys. Rev. B 35, 3675 (1987).

20 G. Hess, T. Hopkins, and Y. Xia, http://meetings.aps.org/link/BAPS.2005.MAR.X34.11

21 A. N. Cherevatova, V. N. Bocharov, T. D. Kolomiitsova, D. N. Shchepkin, and K. G. Tokhadze, Low Temp. Phys. **36**, 439 (2010).

22 B. I. Swanson and L. H. Jones, J. Chem. Phys. 74, 3205 (1981).

23 Yu. A. Tsyganenko, A. A. Tsyganenko, and K. S. Smirnov, Vibr. Spectros. **6**, 15 (1993); Yu. A. Tsyganenko *et al*., *ibid*. **13**, 11 (1996).

24 B. N. J. Persson and R. Ryberg, Phys. Rev. B **24**, 6954 ((1981).

25 T. L. Hill, "An Introduction to Statistical Thermodynamics" (Dover, New York, 1986), p. 376.

Figure Captions

Fig. 1. A typical spectrum in the bilayer region at 105.9 K. The peak near 1004 cm^{-1} is due to SF_6 in the first layer and the peak near 1319 cm^{-1} is due to CF_4 in the second layer. The noisy band between 1250 and 1290 cm^{-1} is where CF_4 gas in the cell strongly attenuates both polarizations.

Fig. 2. (A) Ellipsometric coverage record for a run at T = 100.6 K. Open squares are on increasing pressure of CF_4 and small solid squares are on decreasing pressure. (B) Collective mode vibrational frequencies *versus* pressure of CF_4 at T = 100.6 K: SF_6 frequency on increasing and decreasing pressure (Open circles and pluses, respectively; left axis). CF_4 frequency on increasing and decreasing pressure (Solid squares and open squares, respectively; right axis).

Fig. 3. SF_6 frequency *versus* temperature at three characteristic points in the isotherms: (A) Saturated SF_6 before admission of CF_4 (open circles); (B) Just before second layer step (solid squares with dashed line); (C) Just after second layer step (solid triangles).

Fig. 4. Plot of film properties *versus* time as CF_4 pressure approaches and leaves saturation: Open squares, effective number of layers from ellipsometry (right axis); solid circles, area of the spectral peak due to SF_6 in the bottom layer (left axis).

Fig. 5. Plot of film properties *versus* time as CF_4 pressure approaches and leaves saturation: Solid squares, effective number of layers from ellipsometry (left axis); open circles, area of the spectral peak at 939 cm^{-1}, attributed to 3-D dissolved SF_6 (right axis).

Fig. 6. Plot of film properties *versus* time as CF_4 pressure approaches and leaves saturation: Open squares, partial pressure of SF_6 (right axis); solid circles (for reference), area of the spectral peak due to SF_6 in the bottom layer (left axis).

Fig. 7. Vibrational frequencies *versus* chemical potential of CF_4 for an isotherm starting with an SF_6 monolayer well below saturation, at T = 111.3 K. Open circles with dashed line, SF_6 frequency on increasing pressure (left axis); solid squares, CF_4 frequency (right axis). In this case the absorption peak for CF_4 in the first layer is observable well before the second layer step.

Fig. 8. ν_{CF4} *versus* ν_{SF6} from simulations on a hexagonal net with nearest neighbor distance 5.03 Å. Lines are fits to calculations for about 132 concentrations each for various values of the parameter Δ. The heavy line is for random distribution (Δ = 0); the lower-left line is for interactions favoring unlike nearest neighbors (large negative Δ/T). The remaining lines are for interactions favoring like nearest neighbors: Dashed, Δ/T = 0.21; solid, Δ/T = 0.26; dash-dot, Δ/T = 0.33; upper-right solid line, large positive Δ/T (where phase separation is limited by the cell size). Solid squares and open circles are experimental data (see text).

Fig. 9. ν_{CF4} and ν_{SF6} *versus* concentration from simulations for Δ/T = 0.21 and nearest neighbor distance a = 4.92 Å, re-scaled as described in the text. Heavy lines are polynomial fits. Dashed lines mark the locations of the free molecular resonances.

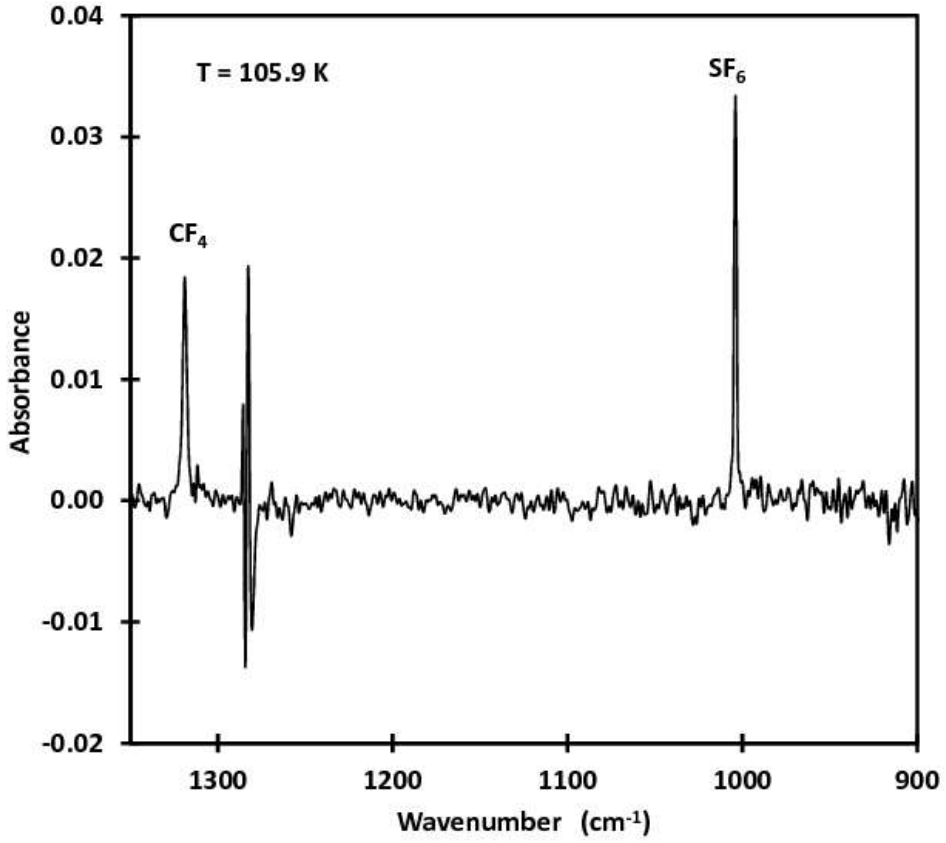

FIGURE 1

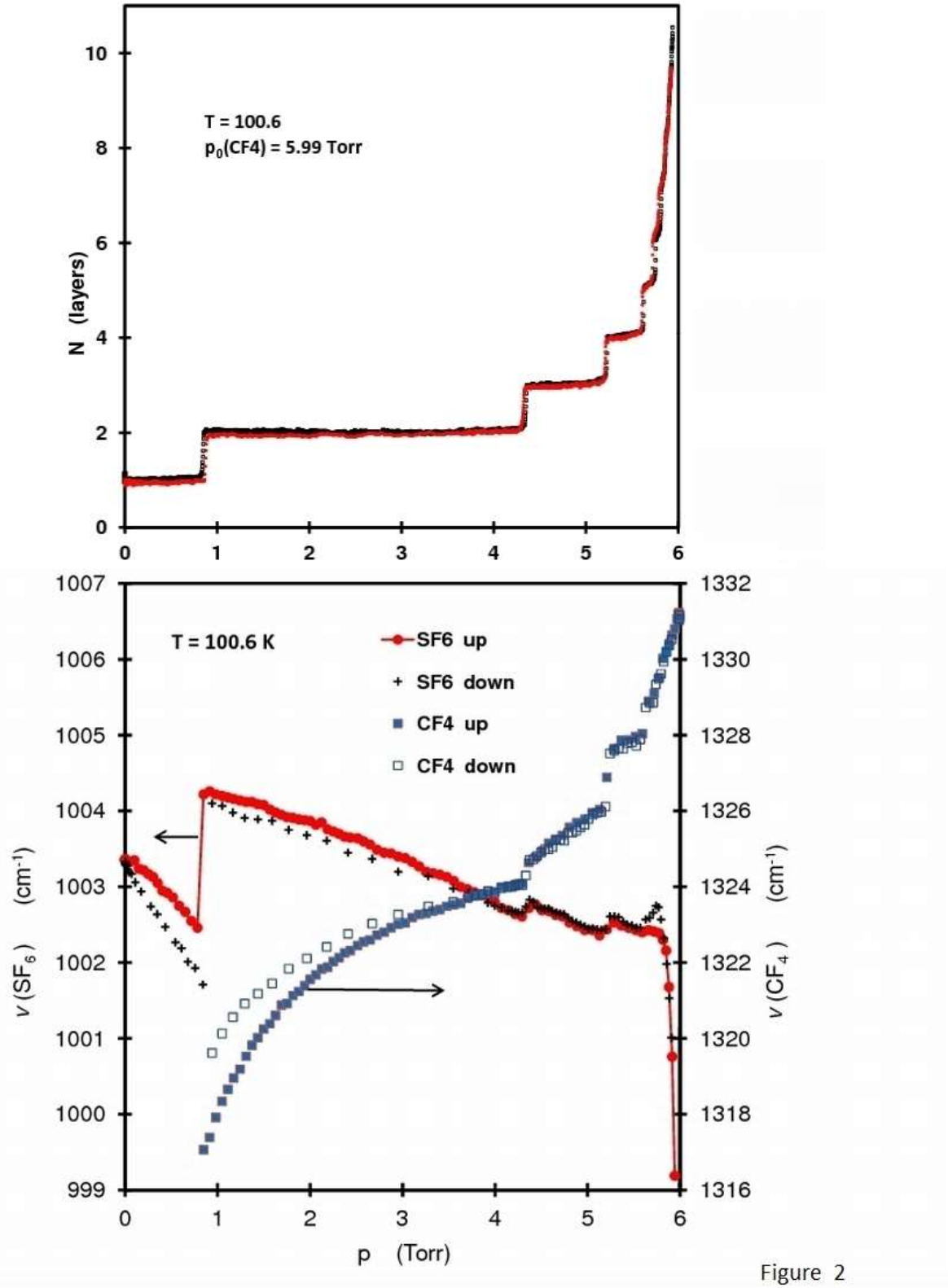

Figure 2

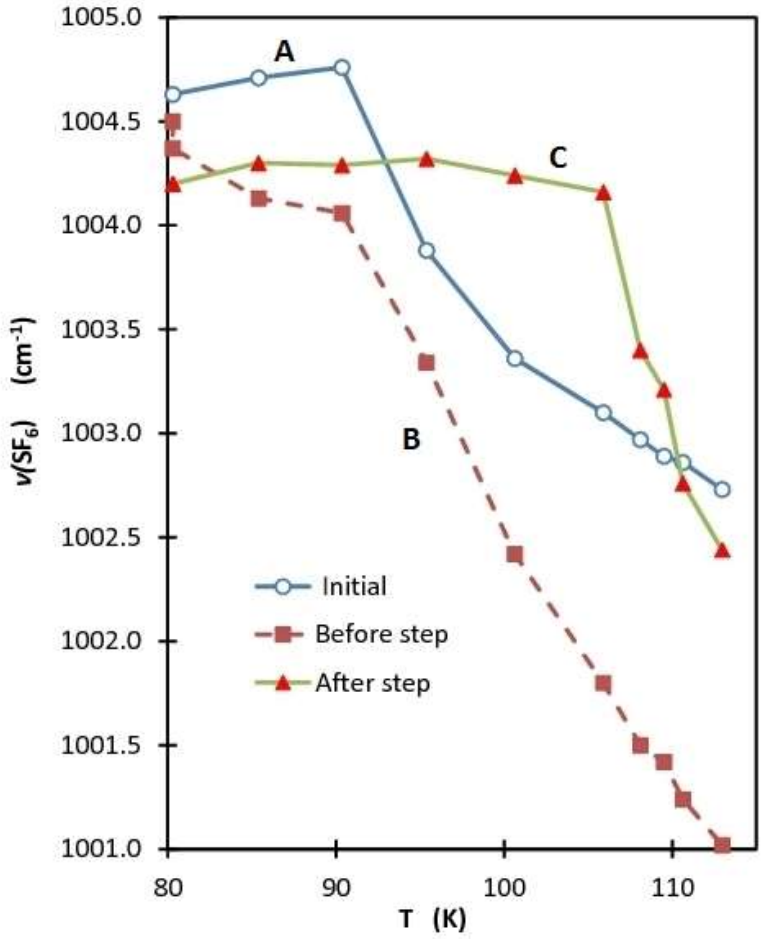

FIGURE 3

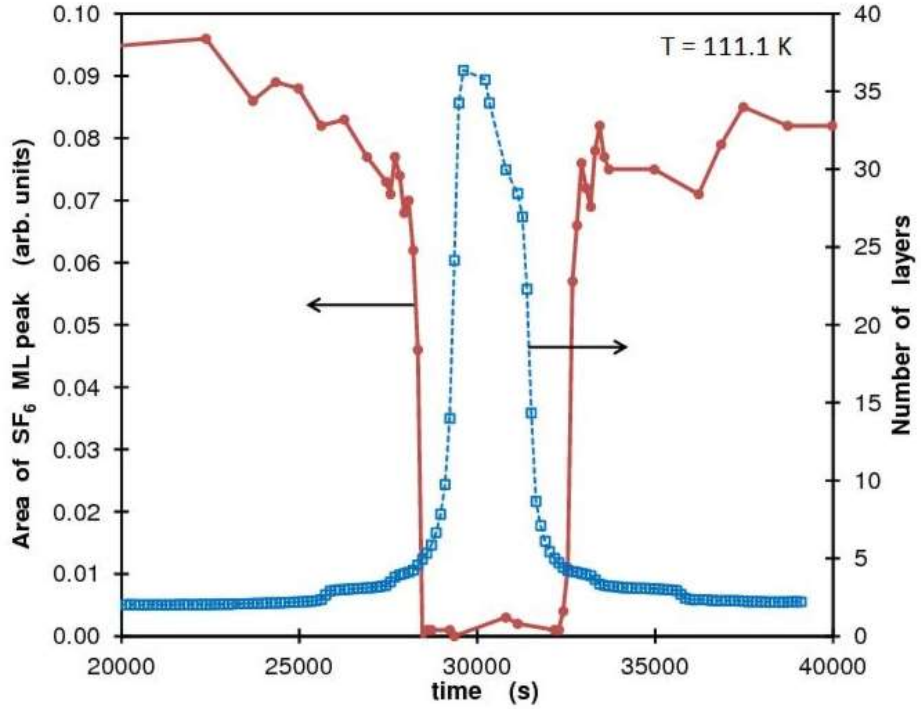

FIGURE 4

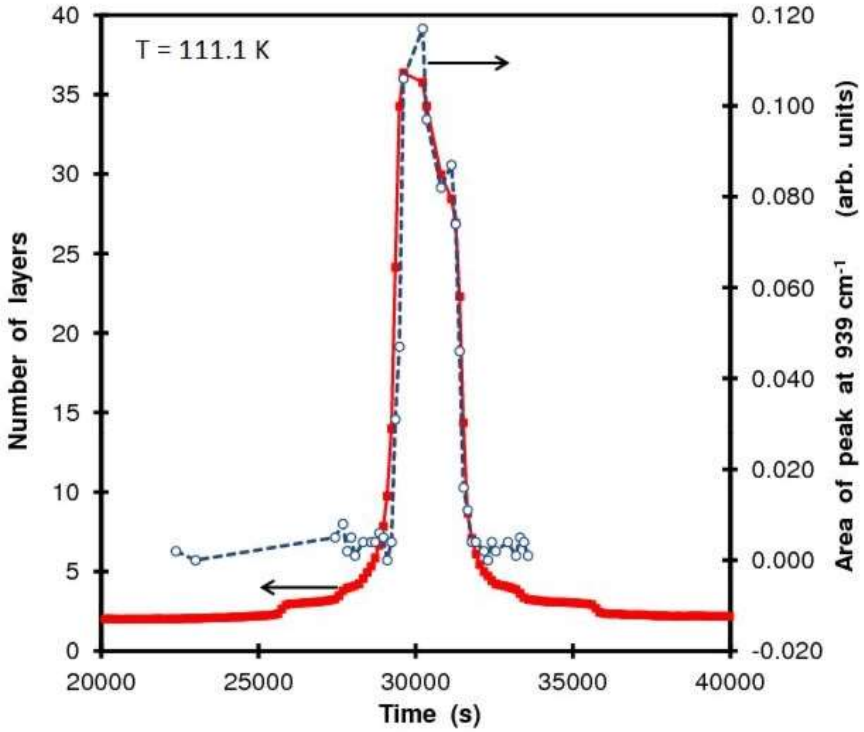

FIGURE 5

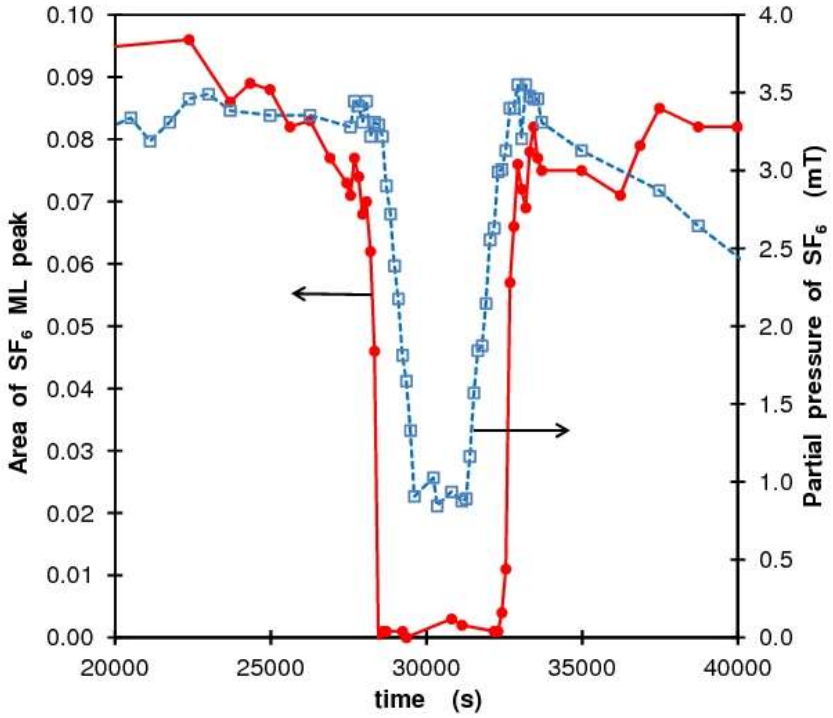

Figure 6

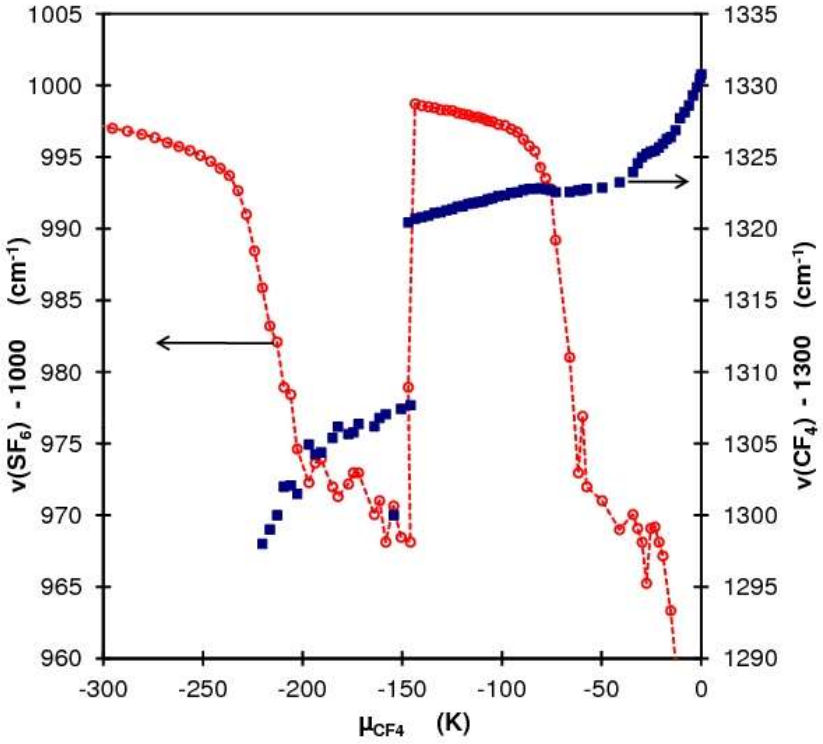

FIGURE 7

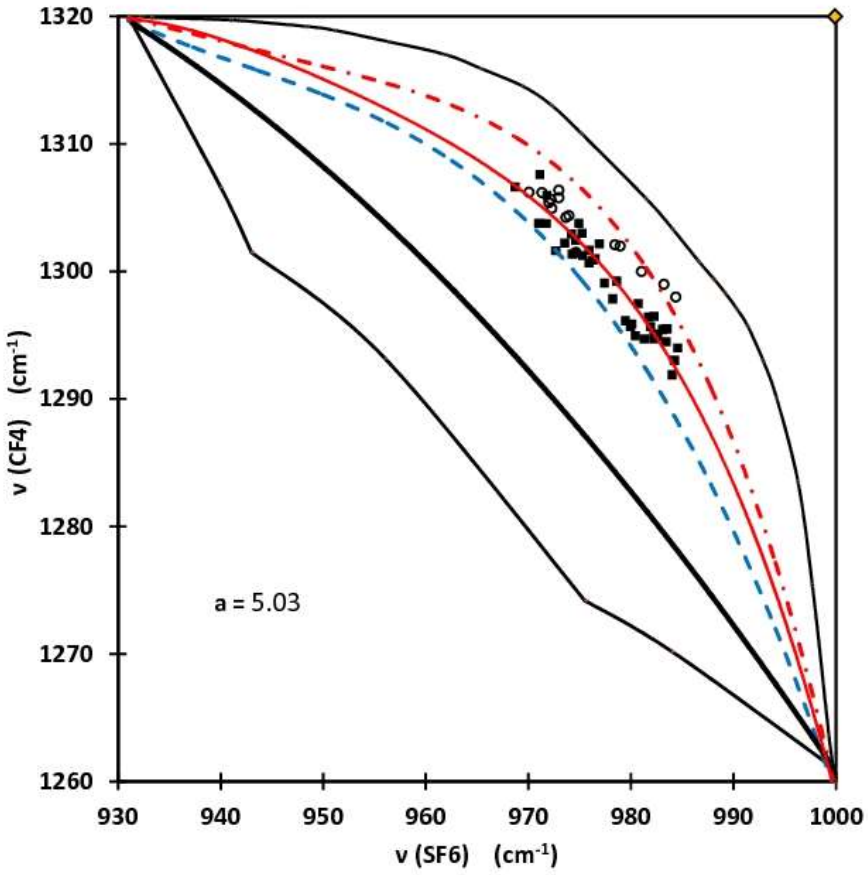

FIGURE 8

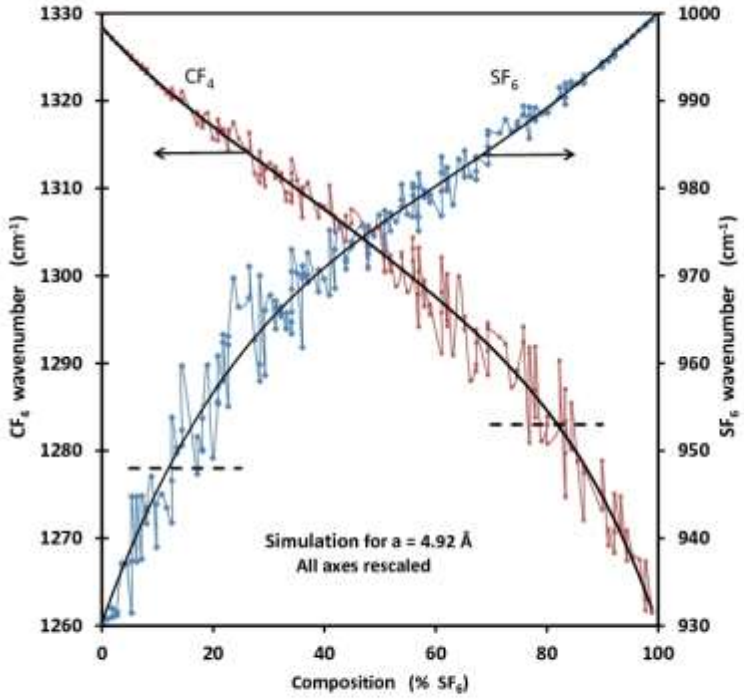

Figure 9

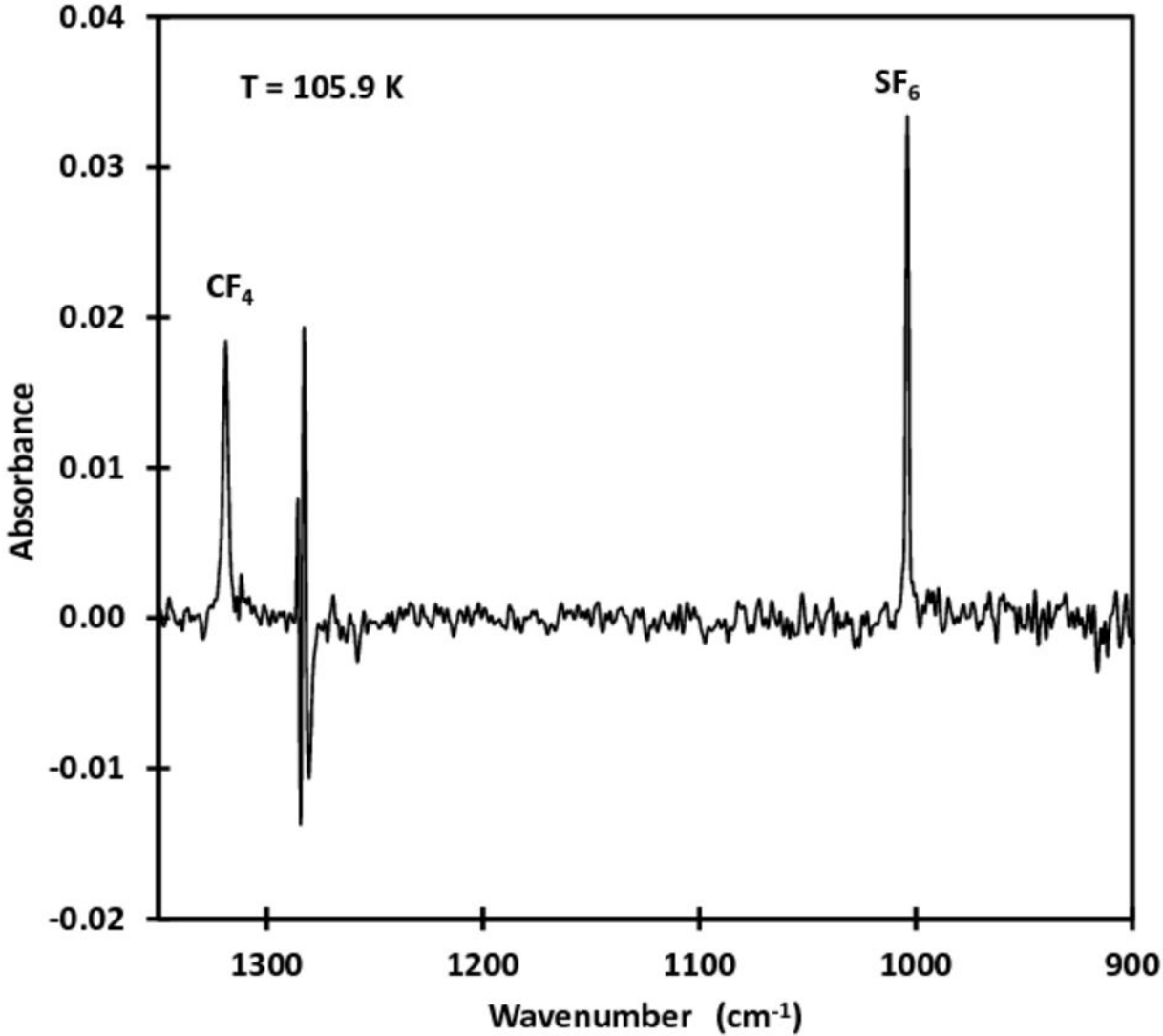

FIGURE 1

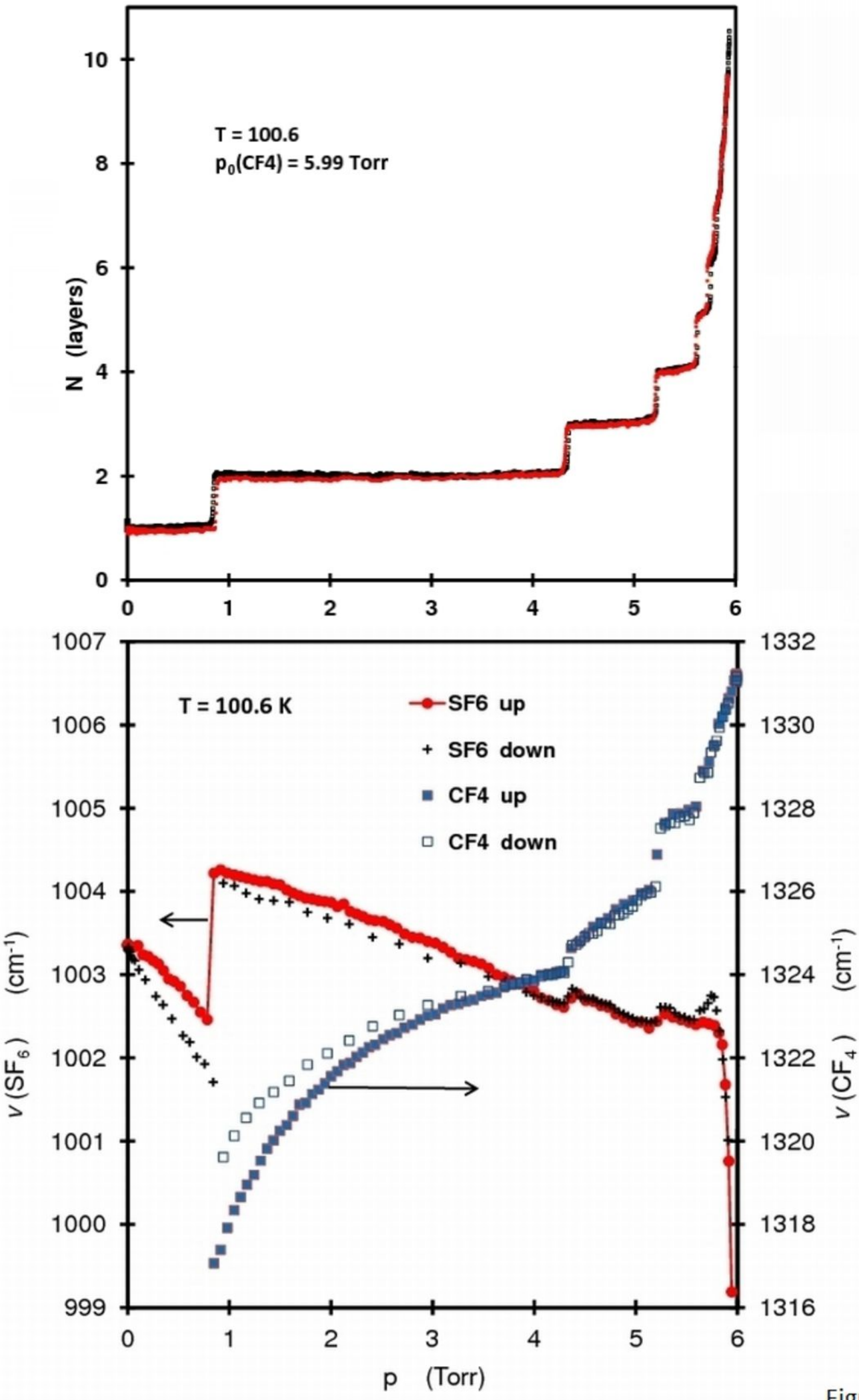

Figure 2

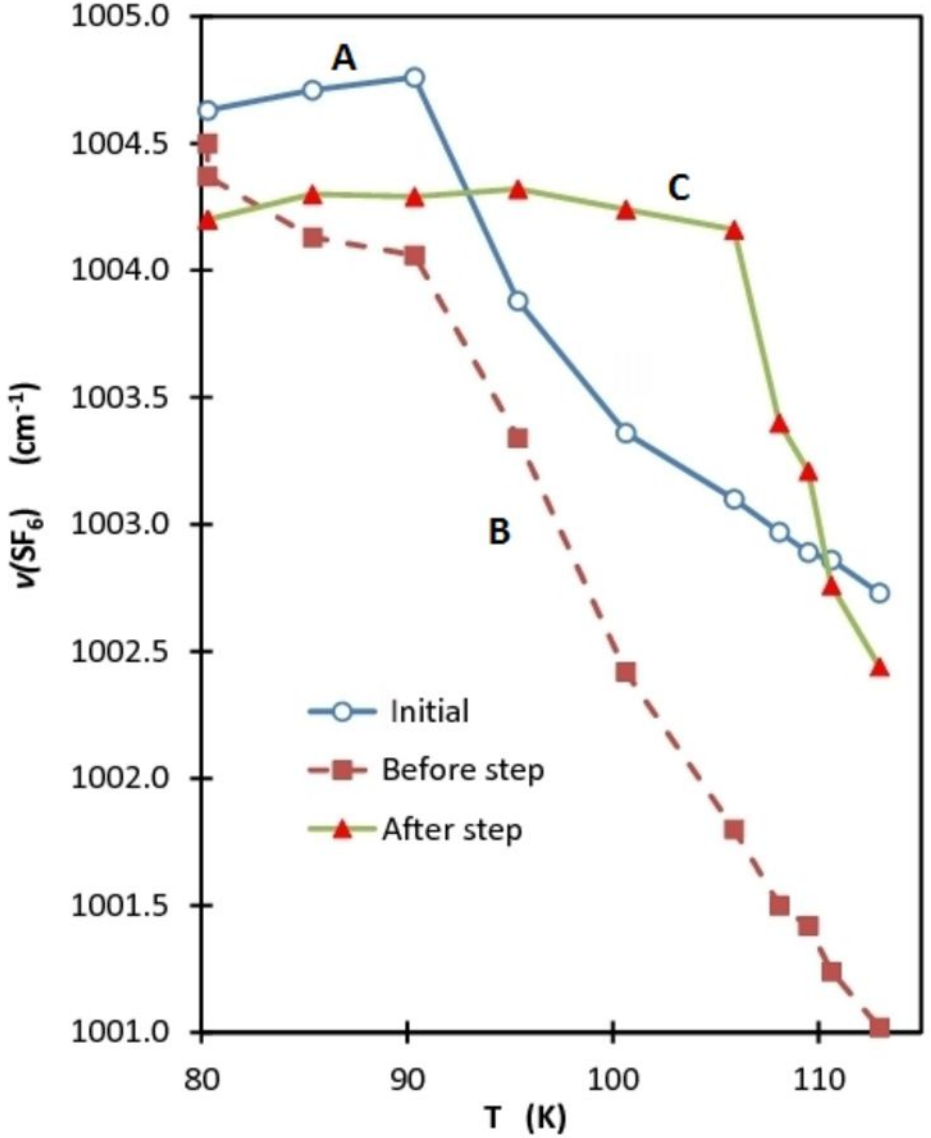

FIGURE 3

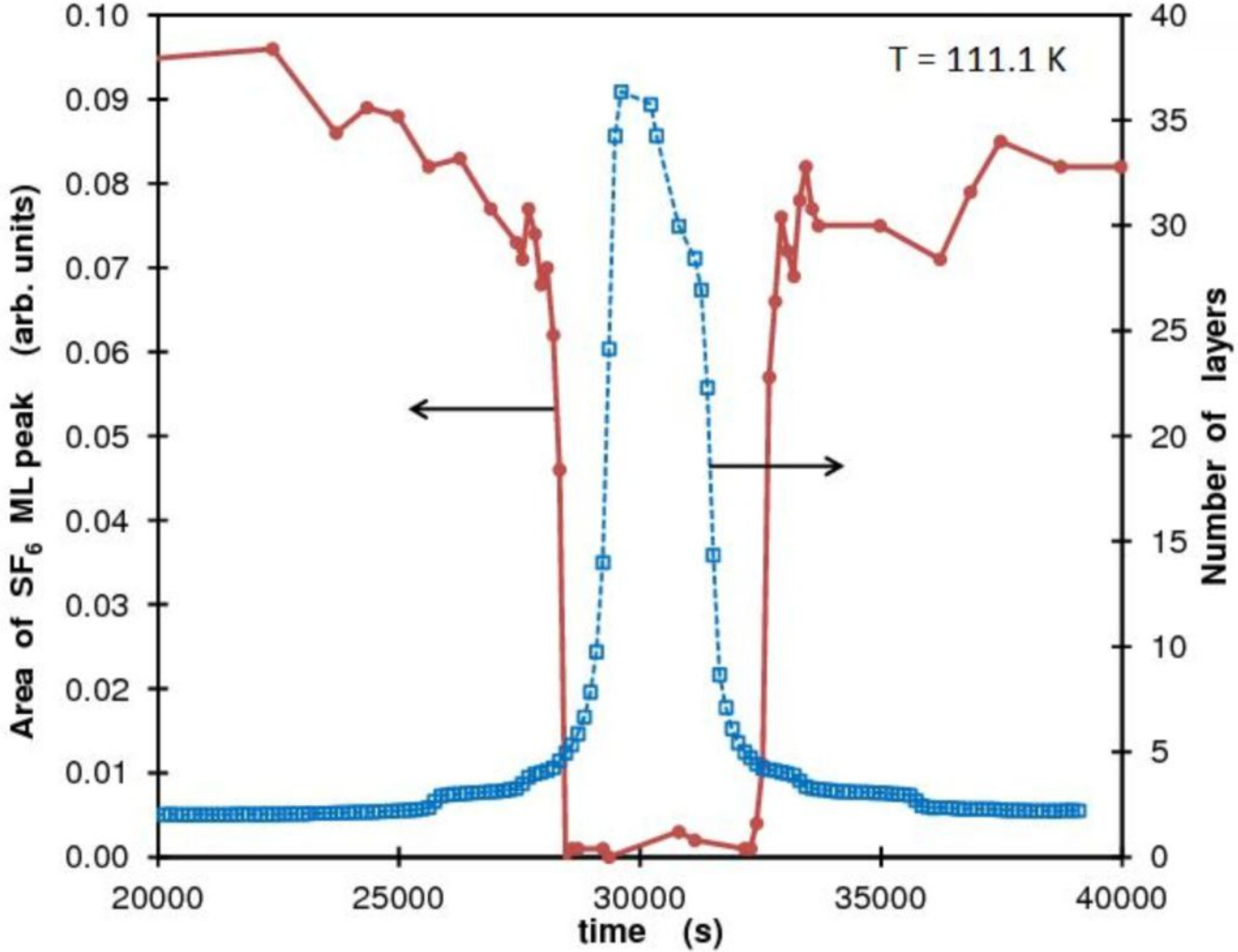

FIGURE 4

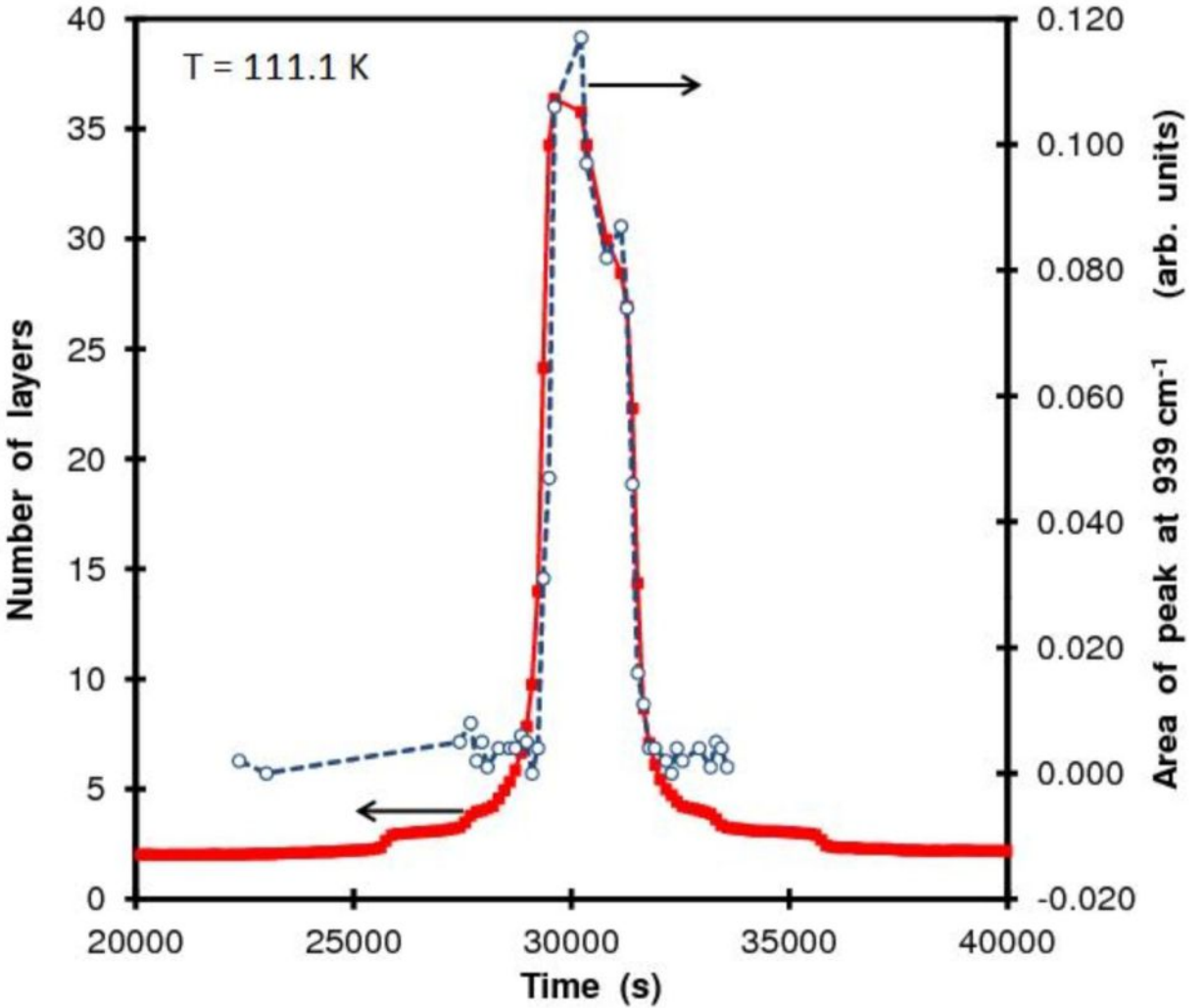

FIGURE 5

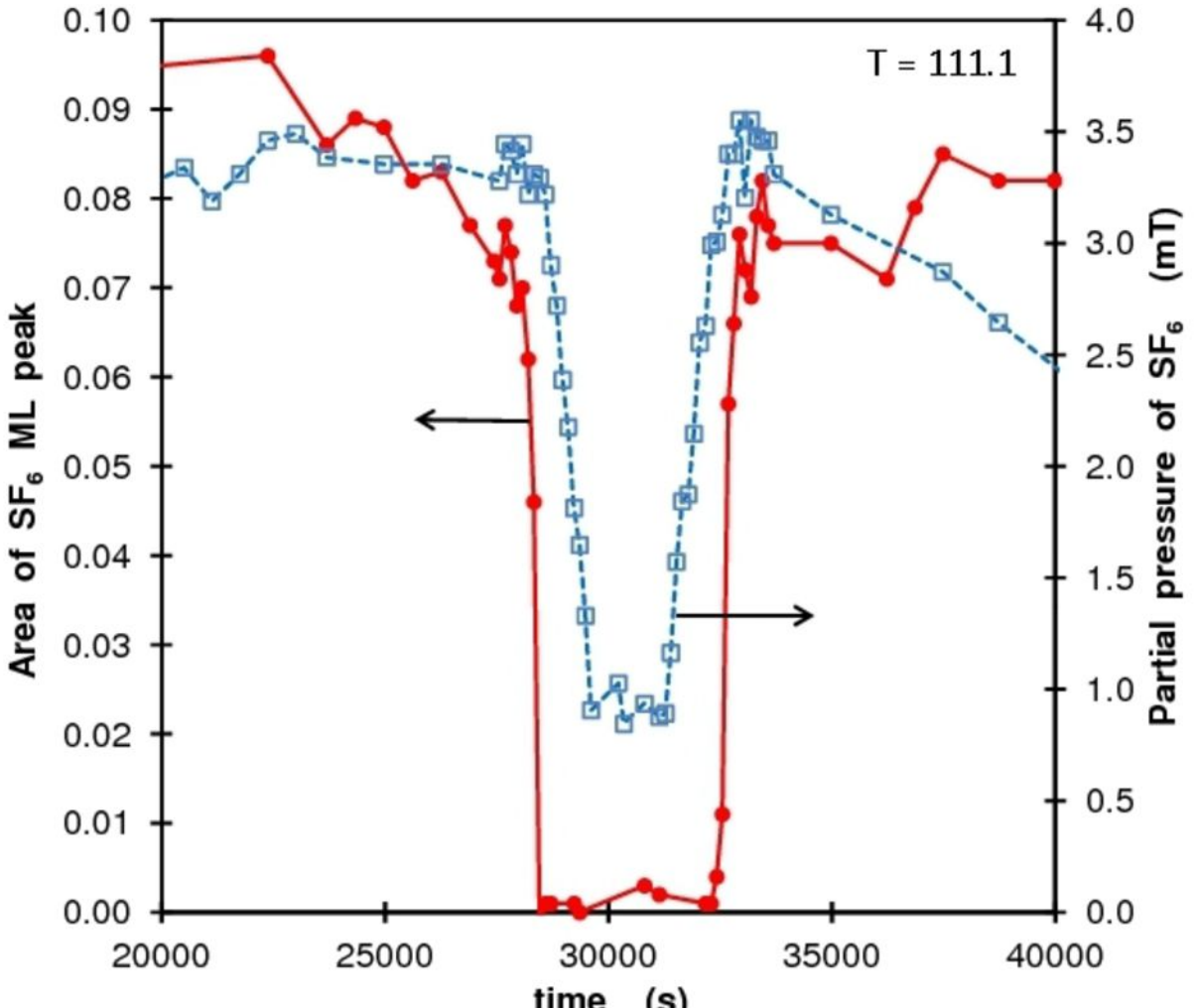

Figure 6

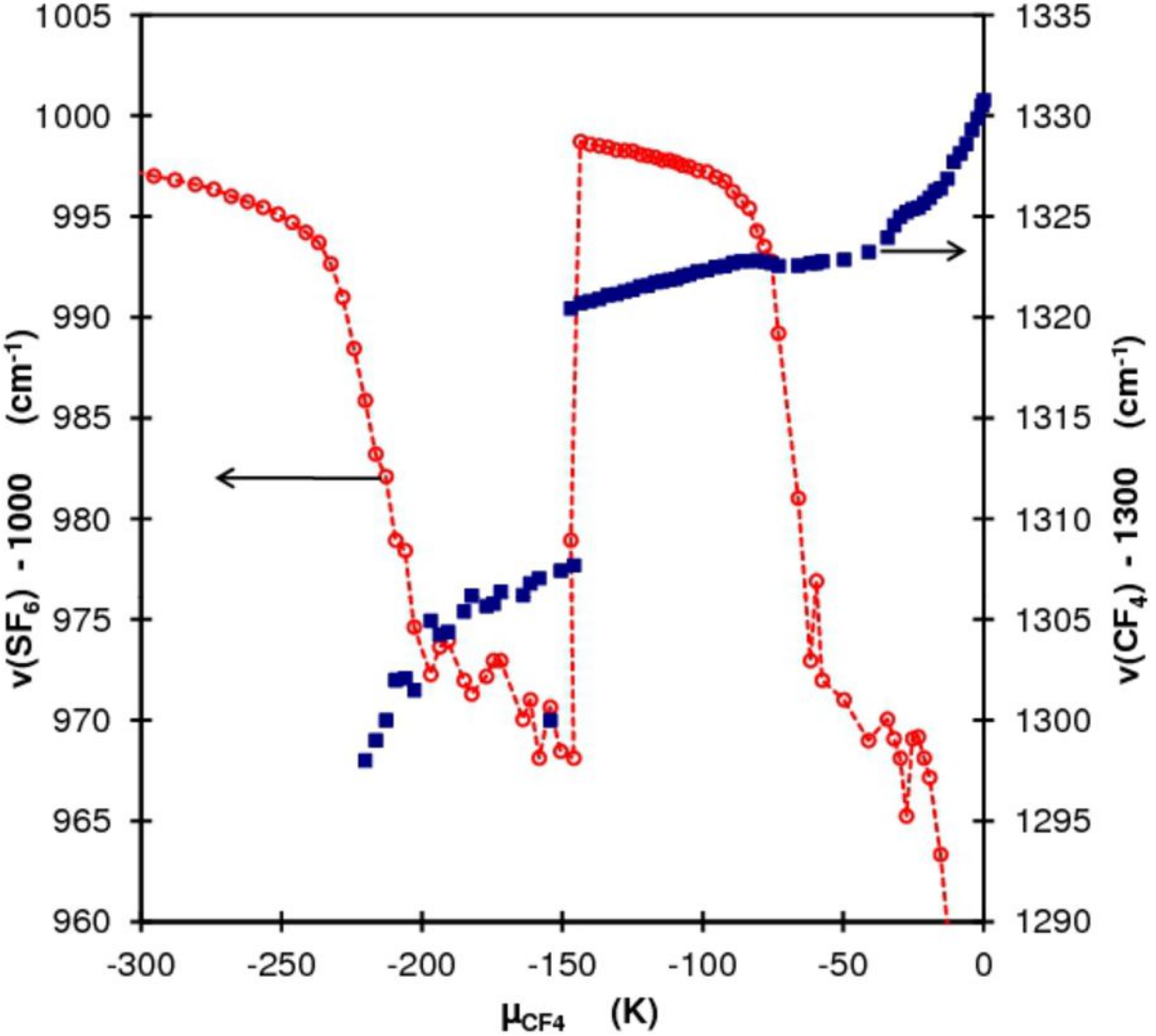

FIGURE 7

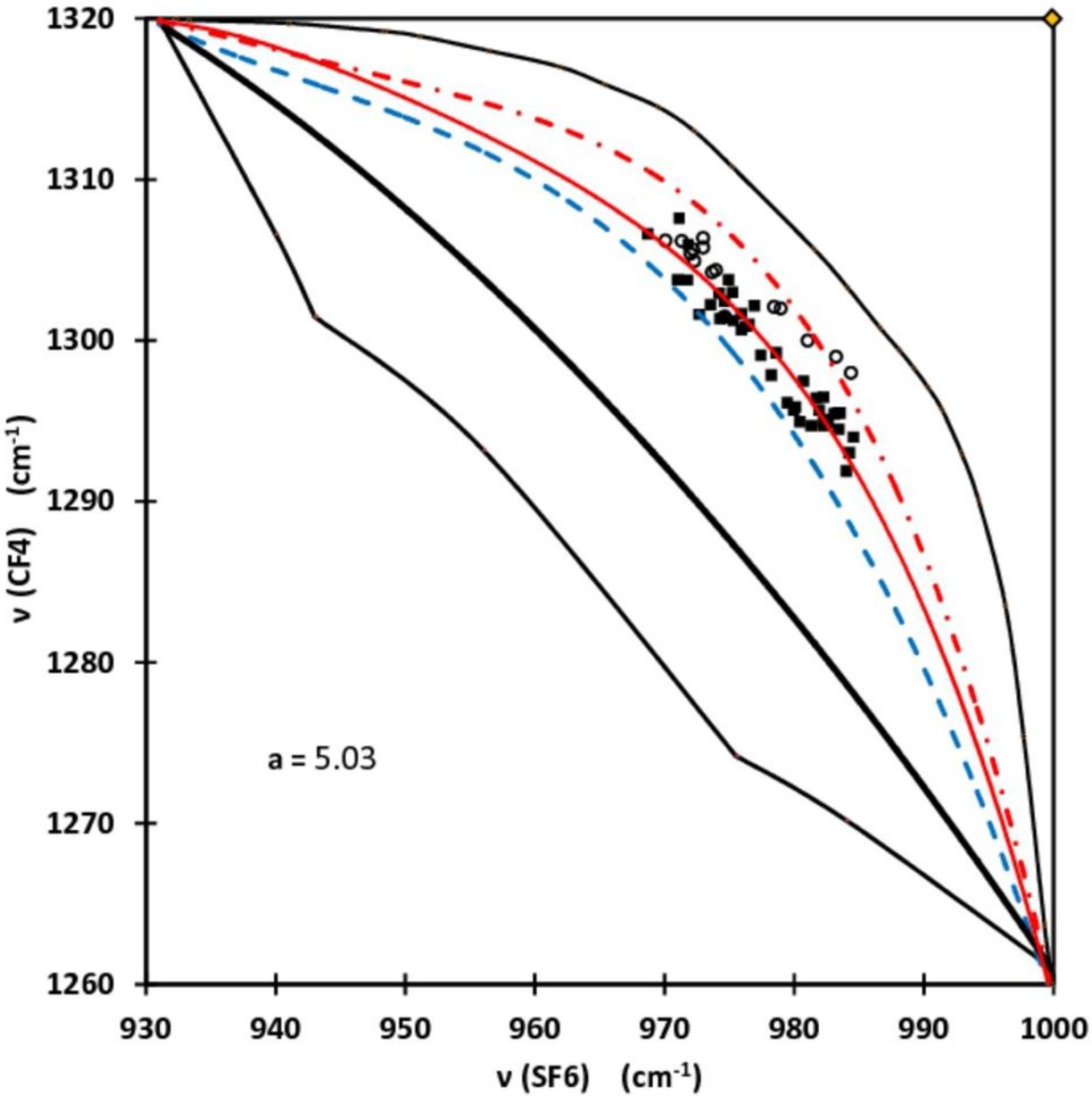

FIGURE 8

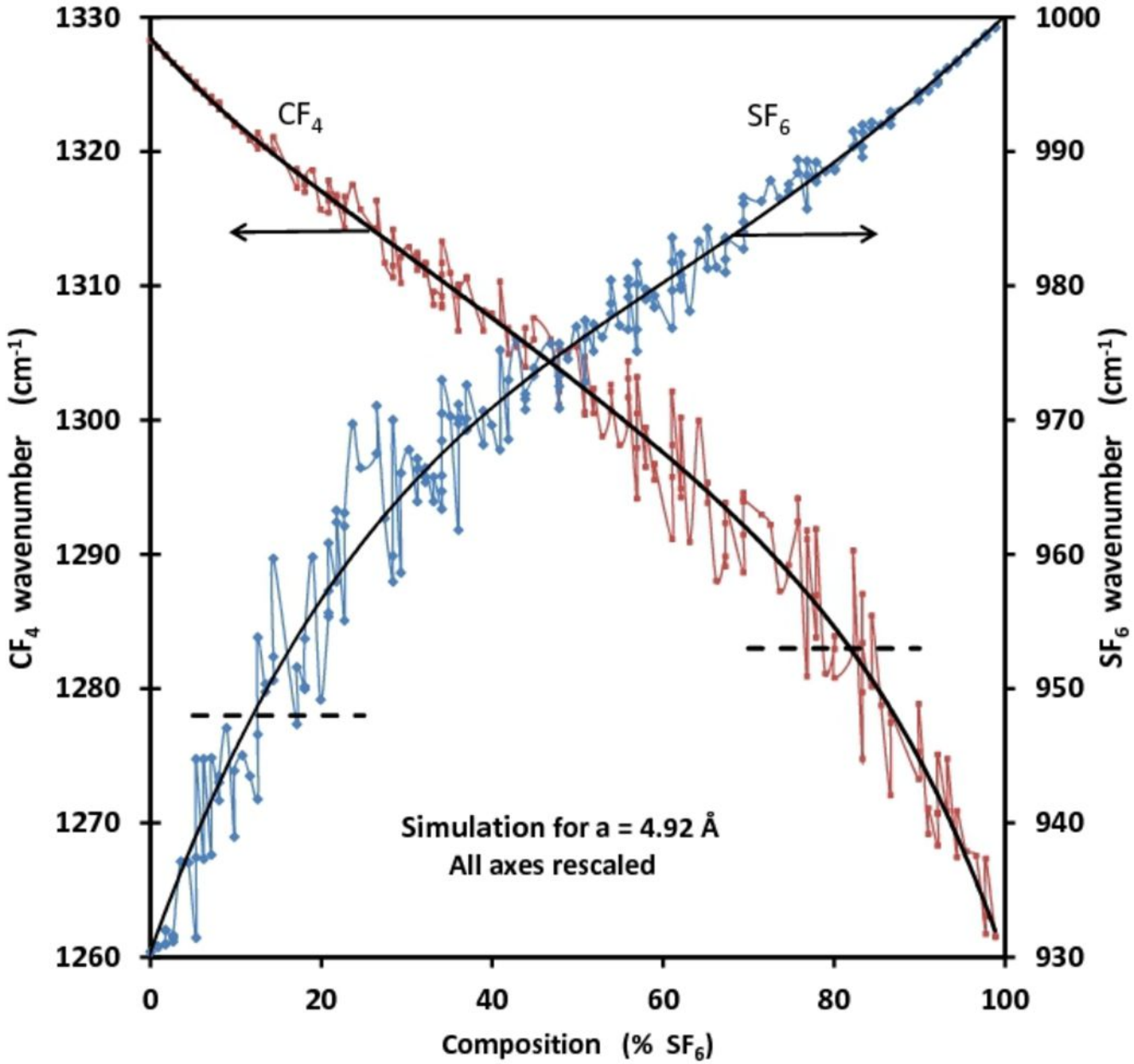

Figure 9